



## Sparse recovery under nonnegativity and sum-to-one constraints

Xiao-Peng Li<sup>a</sup>, Chi-Sing Leung<sup>b,\*</sup>, Hing Cheung So<sup>b</sup>

<sup>a</sup> College of Electronics and Information Engineering, Shenzhen University, Shenzhen, China

<sup>b</sup> Department of Electrical Engineering, City University of Hong Kong, Hong Kong Special Administrative Region of China



### ARTICLE INFO

**Keywords:**

Sparse recovery  
Nonnegative  
Sum-to-one  
Sparse index tracking  
Hyperspectral unmixing

### ABSTRACT

Sparse recovery under nonnegativity and sum-to-one constraints is a special form of the linear regression problem, where the solution is required to simultaneously satisfy sparsity, nonnegativity, and sum-to-one restraints. Existing algorithms for this task mainly utilize the penalty technique to convert the sparsity constraint into a regularization term. Therefore, the sparsity is determined via tuning the associated penalty parameter, which is time-consuming in practice. This paper exploits projected gradient descent to directly tackle the constrained problem without involving the penalty parameter and  $\ell_0$ -norm approximation. The addition of the  $\ell_0$ -norm constraint with a specific upper bound enables the proposed algorithm to *explicitly control* sparsity. The developed method is termed as modified iterative hard thresholding (MIHT), comprised of two iterative steps, namely, gradient descent and nonconvex projection. For the latter, the constraint set consists of the  $\ell_0$ -norm, nonnegativity, and sum-to-one constraints. We devise an efficient algorithm to address the nonconvex projection and then prove that this method produces an optimal solution. Furthermore, we establish the convergence of the MIHT, including objective value and variable sequence. Numerical experiments using financial and hyperspectral data demonstrate that the MIHT is superior to state-of-the-art methods in terms of prediction error and recovery accuracy.

### 1. Introduction

Sparse recovery (a.k.a. compressed sensing) aims at restoring a sparse vector from an observed signal based on a given basis [1–4], and its applications include image processing [5,6], medical imaging [7], radar [8], action recognition [9], and machine learning [10]. In practice, several problems possess further additional properties, namely, nonnegativity and sum-to-one. For instance, in index tracking [11,12], the decision variables represent the investment percentages in various assets, necessitating that their values should be nonnegative. Additionally, the sum of these percentages should equal 1. A similar requirement for the two constraints is also observed in the hyperspectral unmixing problem [13].

#### 1.1. Prior art

Given a vector  $\mathbf{y} = \mathbf{Ax}$ , the process of sparse recovery subject to nonnegativity and sum-to-one constraints can be expressed as the following optimization problem

$$\min_{\mathbf{x}} \|\mathbf{Ax} - \mathbf{y}\|_2^2 \quad \text{s.t. } \mathbf{x} \geq 0, \|\mathbf{x}\|_0 \leq S, \mathbf{1}^T \mathbf{x} = 1, \quad (1)$$

\* Corresponding author.

E-mail addresses: [x.p.li@szu.edu.cn](mailto:x.p.li@szu.edu.cn) (X.-P. Li), [epleungc@cityu.edu.hk](mailto:epleungc@cityu.edu.hk) (C.-S. Leung), [hcso@ee.cityu.edu.hk](mailto:hcso@ee.cityu.edu.hk) (H.C. So).

where  $\mathbf{y} \in \mathbb{R}^m$ ,  $\mathbf{A} \in \mathbb{R}^{m \times n}$  is a known measurement matrix,  $S > 0$  controls the sparsity of  $\mathbf{x}$ , while  $\|\cdot\|_2$  and  $\|\cdot\|_0$  are  $\ell_2$ -norm and  $\ell_0$  norm, respectively. In this work, we refer to task (1) as sparse recovery under nonnegativity and sum-to-one constraints (SR-NS). The inclusion of the  $\ell_0$ -norm constraint renders SR-NS nonconvex and NP-hard [6], such that only a sub-optimal solution can be found in polynomial time.

To tackle SR-NS, works [14,15] decompose (1) into two independent subproblems, i.e., sparse selection and sum-to-one optimization. Specifically, [15] formulates the two subtasks as

$$\min_{\mathbf{x}} \|\mathbf{Ax} - \mathbf{y}\|_2^2 \quad \text{s.t. } \mathbf{x} \geq 0, \|\mathbf{x}\|_0 \leq S, \quad (2a)$$

$$\min_{\bar{\mathbf{x}}} \|\bar{\mathbf{A}}\bar{\mathbf{x}} - \mathbf{y}\|_2^2 \quad \text{s.t. } \bar{\mathbf{x}} \geq 0, \mathbf{1}^T \bar{\mathbf{x}} = 1, \quad (2b)$$

where  $\bar{\mathbf{x}} \in \mathbb{R}^S$  is a condensed vector formed by selecting specific entries from  $\mathbf{x}$ , and  $\bar{\mathbf{A}} \in \mathbb{R}^{m \times S}$  is composed of the corresponding columns from  $\mathbf{A}$ . Although (2a) is still an NP-hard problem, a satisfactory solution can be attained using the nonnegative orthogonal matching pursuit algorithm [16,17]. In addition, (2b) is a convex optimization problem and thus its global optimal solution can be found. Therefore, this approach is able to seek a solution that satisfies the three constraints, however it is not clear whether the solution is the minimizer of SR-NS.

Another popular strategy is to exploit the penalty approach that is widely adopted in the classic sparse recovery [18]. Specifically, it converts the  $\ell_0$ -norm constraint into a regularization term in the objective function:

$$\min_{\mathbf{x}} \|\mathbf{Ax} - \mathbf{y}\|_2^2 + \lambda \|\mathbf{x}\|_0 \quad \text{s.t. } \mathbf{x} \geq 0, \mathbf{1}^T \mathbf{x} = 1, \quad (3)$$

where  $\lambda > 0$  is a penalty parameter trading off the fitting error and sparsity. Then,  $\ell_0$ -norm is substituted by its approximation function, such as  $\ell_1$ -norm [19] and log function [20]. Compared with the  $\ell_1$ -norm, the log function can enforce stronger sparsity-promoting and less biased solutions [20]. In [21], the  $\ell_1$ -norm is employed to handle (3), where SR-NS is reformulated as the famous least absolute shrinkage and selection operator (LASSO) [22,23] with a nonnegativity constraint:

$$\min_{\mathbf{x}} \|\mathbf{Ax} - \mathbf{y}\|_2^2 + \lambda \|\mathbf{x}\|_1 \quad \text{s.t. } \mathbf{x} \geq 0, \quad (4)$$

where  $\|\cdot\|_1$  is the  $\ell_1$ -norm. It is worth noting that the sum-to-one restriction is not involved as the nonnegativity and sum-to-one constraints make the  $\ell_1$ -norm term to be a constant, i.e., 1. This strategy that discards the sum-to-one constraint is also employed in hyperspectral unmixing [24–26]. Whilst it can attain an acceptable solution, the result might deviate from the ground truth. To handle this issue, weighted  $\ell_1$ -norm [27] is suggested to deal with (3) in [28,29]. For instance, Shu et al. [28] reformulate (3) as

$$\min_{\mathbf{x}} \|\mathbf{Ax} - \mathbf{y}\|_2^2 + \lambda_1 \|\mathbf{w}^T \mathbf{x}\|_1 + \lambda_2 \|\mathbf{x}\|_2 + \lambda_3 \|\mathbf{x} - \hat{\mathbf{x}}\|_1 \quad \text{s.t. } \mathbf{x} \geq 0, \mathbf{1}^T \mathbf{x} = 1, \quad (5)$$

where  $\lambda_1 > 0$ ,  $\lambda_2 > 0$ , and  $\lambda_3 > 0$  are penalty parameters,  $\mathbf{w} \in \mathbb{R}^n$  is a reweighted vector, and  $\hat{\mathbf{x}} \in \mathbb{R}^n$  is a reference vector. Then, the augmented Lagrangian method [30] is adopted as the solver of the resultant problem. It is worth mentioning that the  $\ell_1$ -norm cannot guarantee the solution to be the sparsest, implying that there are lots of very small values of  $x_i$  rather than zero. Therefore, a truncation operation is required for the solution to attain the target sparsity level, resulting in the sum being not equal to 1. Furthermore, a continuous and differentiable function is devised to approximate  $\ell_0$ -norm [31,32]:

$$\rho_{p,\zeta}(\mathbf{x}) = [\rho_{p,\zeta}(x_i)] = \left[ \frac{\log(1 + |x_i|/p)}{\log(1 + \zeta/p)} \right], \quad (6)$$

where  $0 < p \ll 1$  and  $\zeta > 0$ . Compared with  $\ell_1$ -norm and weighted  $\ell_1$ -norm,  $\rho_{p,\zeta}(\cdot)$  is able to obtain a nearly sparse solution. Based on this surrogate function, (3) is rewritten as [32]

$$\min_{\mathbf{x}} \|\mathbf{Ax} - \mathbf{y}\|_2^2 + \lambda \mathbf{1}^T \rho_{p,\zeta}(\mathbf{x}) \quad \text{s.t. } \mathbf{x} \geq 0, \mathbf{1}^T \mathbf{x} = 1, \quad (7)$$

which is then tackled by the majorization-minimization approach [33]. Furthermore, other nonconvex surrogates, e.g.,  $\tanh(\frac{x^2}{2\sigma^2})$  and  $\frac{|x|}{|x| + \sigma}$  with  $\sigma > 0$ , are proposed to approximate  $\ell_0$ -norm in sparse recovery [18,34,35]. Due to the approximation gap, the corresponding algorithms yield biased estimates. Note that the above-mentioned methods require tuning penalty parameters to determine the sparsity.

## 1.2. Motivations and contributions

In practical applications, it is necessary to search for a solution with a specified sparsity, which represents certain significance. For instance, in sparse index tracking, the sparsity indicates the number of selected assets. If an investor has a clear demand for choosing  $S$  stocks to track the market index, the sparsity should equal  $S$ . Moreover, in hyperspectral unmixing [36], controlling the sparsity is able to restrict the number of spectral signatures of each pixel. However, the penalty approach requires tweaking the regularization parameter for the desired sparsity, which is a time-consuming procedure. As a result, there is a need for devising an algorithm capable of efficiently solving (1).

Referring to (1), a feasible strategy to meet this requirement is to adopt the projected gradient descent algorithm [20,37,38], but the challenge is how to find a solution simultaneously meeting the three constraints based on an optimization problem. Another challenge is that the corresponding algorithm should have convergence guarantee with theoretical analysis.

In this paper, we directly address (1) without relying on the penalty approach or approximation function. Therefore, our method can precisely control sparsity through the specified upper bound  $S$ . We adopt projected gradient descent as the solver to develop a modified iterative hard thresholding (MIHT) algorithm. Specifically, the MIHT consists of two procedures, viz. gradient descent and nonconvex projection. The latter is formulated by a nonconvex set, including  $\ell_0$ -norm, nonnegativity, and sum-to-one constraints. We then derive an efficient implementation for the nonconvex projection based on the Karush–Kuhn–Tucker (KKT) condition and then prove the optimality of its solution. In addition, we analyze the convergence behavior of MIHT, including objective value and variable sequence. Furthermore, experimental results on sparse index tracking and hyperspectral unmixing exhibit the superior performance of MIHT over the state-of-the-art approaches in terms of prediction error. Our main contributions are summarized as:

- (i) The proposed MIHT tackles SR-NS without using the penalty method and approximation function. Therefore, the suggested method is able to explicitly control the sparsity.
- (ii) This paper derives an efficient algorithm for the nonconvex projection in the MIHT. Besides, this method is proven to obtain an optimal solution.
- (iii) The convergence behavior of the MIHT is analyzed, ensuring that both the objective value and variable sequence converge.
- (iv) The devised algorithm exhibits superior performance compared to the competing methods in sparse index tracking and hyperspectral unmixing.

The rest of this paper is organized as follows. We develop MIHT and then prove that the proposed algorithm for nonconvex projection yields an optimal solution in Section 2. Moreover, the convergence and computational complexity of the MIHT are analyzed. In Section 3, numerical results based on sparse index tracking and hyperspectral unmixing are presented. Finally, conclusion is included in Section 4.

## 2. Algorithm development

### 2.1. Proposed method

Inspired by [20] in which projected gradient descent is exploited to handle convolutional transform learning, we directly solve (1) via the following iterative procedure:

$$\mathbf{z}^{t+1} = \mathbf{x}^t - 2\eta \mathbf{A}^T(\mathbf{Ax}^t - \mathbf{y}), \quad (8a)$$

$$\mathbf{x}^{t+1} = P_C(\mathbf{z}^{t+1}), \quad (8b)$$

where  $\eta > 0$  is the step-size and  $P_C(\mathbf{z})$  is a projection operator. The step (8a) corresponds to the gradient descent, which can be easily derived and implemented. In (8b),  $P_C(\mathbf{z})$  is defined as

$$\min_{\mathbf{x}} \|\mathbf{z} - \mathbf{x}\|_2^2 \quad \text{s.t. } \mathbf{x} \geq 0, \mathbf{1}^T \mathbf{x} = 1, \|\mathbf{x}\|_0 \leq S. \quad (9)$$

Herein, we denote  $\mathbf{x}$  as the output of the projection to avoid reuse of notation. To address (9), we first sort  $\mathbf{z}$  in descending order to get  $\hat{\mathbf{z}}$ . From  $s = 1, 2, \dots, S$ , we seek  $\mathbf{x}$  in an iterative manner:

$$\mu_s = \frac{2 \left( \sum_{i=1}^s \hat{z}_i - 1 \right)}{s}, \quad (10a)$$

$$\hat{x}_i = \begin{cases} \hat{z}_i - \frac{\mu_s}{2}, & \text{for } i \in [1, s], \\ 0, & \text{otherwise.} \end{cases} \quad (10b)$$

This process will terminate when either  $s = S$  or  $\hat{z}_{s+1} \leq \mu_s/2$  is satisfied. Once  $\hat{\mathbf{x}}$  is obtained,  $\mathbf{x}$  can be found by reinstating the order of  $\hat{\mathbf{x}}$ . From (10a), (10b) and the termination condition of  $s = S$ , it is apparent that  $\mathbf{x}$  meets the sum-to-one and sparsity constraints. In addition, the nonnegative constraint is ensured by the second stopping condition. This is because  $\mu_s \leq \mu_{s+1}$  and  $\hat{z}_{s+1} \leq \mu_s/2 \leq \mu_{s+1}/2$ . Furthermore, we establish  $\hat{z}_s \geq \mu_s/2$  in Lemma 1. Therefore,  $\hat{z}_{s+1} \leq \mu_s/2$  guarantees the nonnegativity of the solution. The details and the optimality of  $P_C(\mathbf{z})$  will be discussed in Section 2.2. Algorithm 1 summarizes the steps for performing  $P_C(\mathbf{z})$ .

The steps of our MIHT are concisely outlined in Algorithm 2, where there are two stopping criteria. The first one is to terminate at  $t = T_{\max}$ , while the MIHT can terminate when the following criterion meets

$$\frac{\|\mathbf{x}^{t+1} - \mathbf{x}^t\|_2^2}{S} \leq 10^{-8}. \quad (11)$$

The MIHT has three parameters, that is, the sparsity  $S$ , step-size  $\eta$  and maximum iteration number  $T_{\max}$ . For  $S$ , it is set as the desired sparsity. It is worth mentioning that when  $S$  is large, the sparsity of the solution may be less than  $S$ . The choice of  $\eta$  is

**Algorithm 1** Projection  $P_C(\mathbf{z})$ .

---

**Input:**  $\mathbf{z}$  and  $S$   
Sort  $\mathbf{z}$  in the descending order to get  $\hat{\mathbf{z}}$   
**for**  $s = 1, \dots, S$  **do**  
 $\mu_s = \frac{2(\sum_{j=1}^s \hat{z}_j - 1)}{s}$  (ensure sum-to-one property)  
**Stop if**  $s = S$  (ensure sparsity property)  
or  $\hat{z}_{s+1} \leq \mu_s/2$  (ensure nonnegative property)  
**end for**  
Suppose that the above for-loop stops at  $s = s'$   
 $\hat{\chi}_i = \begin{cases} z_i - \frac{\mu_s}{2}, & \text{if } i \in [1, s'], \\ 0, & \text{otherwise.} \end{cases}$   
Restore  $\hat{\chi}$  to get  $\chi$   
**Output:**  $\chi$

---

**Algorithm 2** MIHT for SR-NS.

---

**Input:**  $\mathbf{A}$ ,  $\mathbf{y}$ ,  $S$ ,  $\eta$  and  $T_{\max}$ .  
**Initialize:** Initialize  $\mathbf{x}^t = \mathbf{0}$ .  
**for**  $t = 1, \dots, T_{\max}$  **do**  
Calculate  $\nabla f(\mathbf{x}^t) = 2\mathbf{A}^T(\mathbf{A}\mathbf{x}^t - \mathbf{y})$ .  
Update  $\mathbf{z}^{t+1} = \mathbf{x}^t - \eta \nabla f(\mathbf{x}^t)$ .  
Compute  $\mathbf{x}^{t+1} = P_C(\mathbf{z}^{t+1})$ .  
**Stop if** stopping criterion is met.  
**end for**  
**Output:**  $\mathbf{x}^{t+1}$

---

suggested as  $(0, \alpha/L]$  with  $0 < \alpha \leq 1$  [39], where  $L$  is the  $L$ -Lipschitz constant of  $f(\mathbf{x})$ . For  $f(\mathbf{x}) = \|\mathbf{Ax} - \mathbf{y}\|_2^2$ ,  $L = \sigma_{\max}$ , where  $\sigma_{\max}$  is the largest eigenvalue of  $\mathbf{A}^T\mathbf{A}$ . On the other hand,  $\eta$  can be determined by backtracking line search [40] at each iteration. Compared with the fixed  $\eta$ , an adaptive  $\eta$  is more practical. For  $T_{\max}$ , our experimental results show that  $T_{\max} = 2000$  is sufficient to ensure convergence.

Although both [34] and MIHT adopt projected gradient descent as the solver, the former handles the classic sparse recovery, while the latter tackles SR-NS. Additionally, the projection in [34] is a one-step update, while MIHT requires an iterative procedure to deal with the projection problem.

## 2.2. Optimal projection $P_C(\mathbf{z})$

To demonstrate that Algorithm 1 attains an optimal solution of (9), we first discuss a simplified version of (9), which does not contain the  $\ell_0$ -norm constraint. We then discuss how Algorithm 1 generates an optimal solution.

### 2.2.1. Properties of projection without $\ell_0$ -norm constraint

To increase the legibility, we assume that  $\mathbf{z}$  is sorted in descending order. We first consider the following convex optimization problem

$$\min_{\chi} \|\mathbf{z} - \chi\|_2^2 \quad \text{s.t. } \chi \geq 0, \mathbf{1}^T \chi = 1, \tag{12}$$

which can help us understand the nature of  $P_C(\mathbf{z})$ .

The Lagrangian of (12) is

$$\mathcal{L}(\chi, \mu, \nu) = \|\mathbf{z} - \chi\|_2^2 + \mu(\mathbf{1}^T \chi - 1) - \nu^T \chi, \tag{13}$$

where  $\mu$  and  $\nu$  are the Lagrange multipliers. Since (12) is convex, the KKT conditions of optimality are sufficient and necessary. They are given by

$$\chi_i^* = \frac{1}{2}(v_i^* - (\mu^* - 2z_i)) \text{ for } i \in [1, n], \tag{14a}$$

$$\sum_i^n \chi_i^* = 1 \text{ and } \chi_i^* \geq 0 \text{ for } i \in [1, n], \tag{14b}$$

$$v_i^* \geq 0 \text{ and } v_i^* \chi_i^* = 0 \text{ for } i \in [1, n]. \tag{14c}$$

From the KKT conditions, we discuss three cases of  $\mu^* - 2z_i$ :

- (i)  $\mu^* - 2z_i < 0$ : From the dual feasibility condition, we attain  $v_i^* \geq 0$ , which results in  $\chi_i^* > 0$ . Moreover, the complementary slackness condition requires  $x_i^* v_i^* = 0$ . As a result, we have  $v_i^* = 0$ , leading to  $\chi_i^* = z_i^* - \mu^*/2$ .
- (ii)  $\mu^* - 2z_i = 0$ : According to the complementary slackness condition, we obtain  $\chi_i^* = v_i^* = 0$ .

**Algorithm 3** Projection without  $\ell_0$ -norm constraint.**Input:**  $\mathbf{z}$ **Assumption:**  $\mathbf{z}$  is sorted.**for**  $s = 1, \dots, n$  **do**

$$\mu_s = \frac{2(\sum_{j=1}^s z_j - 1)}{s}.$$

**Stop** if  $s = n$  or  $\hat{z}_{s+1} \leq \mu_s/2$ .**end for**Suppose that the above for-loop stops at  $s = s^*$ .

$$\hat{z}_i = \begin{cases} z_i - \frac{\mu^*}{2}, & \text{if } i \in [1, s^*], \\ 0, & \text{otherwise.} \end{cases}$$

Restore  $\hat{\mathbf{x}}$  to get  $\mathbf{x}$ .**Output:**  $\mathbf{x}$ 

- (iii)  $\mu^* - 2z_i > 0$ : It must hold that  $v_i^* \geq \mu - z_i > 0$  due to the primal feasibility:  $\chi_i^* \geq 0$ . Therefore,  $v_i^* > 0$  holds and then necessarily  $\chi_i^* = 0$  according to the complementary slackness condition.

We first consider a simple case which is  $\mu^* - 2z_i < 0$  for  $i \in [1, n]$ . In this case,  $\|\mathbf{x}\|_0 = n$  and we can set

$$\chi_i^* = z_i - \frac{\mu^*}{2} \text{ for } i \in [1, n], \quad (15a)$$

$$\mu^* = \frac{2(\sum_{i=1}^n z_i - 1)}{n}, \quad (15b)$$

$$\chi_i^* > 0, v_i^* = 0, \text{ and } v_i^* \chi_i^* = 0 \text{ for } i \in [1, n]. \quad (15c)$$

It is apparent that (15) implies (14).

We then consider that  $\|\mathbf{x}\|_0 = s^* < n$ . Since  $z_i$ 's are sorted in descending order,  $\mu^* - 2z_i$  for  $i \in [1, s^*]$  are less than zero. Hence, we have

$$\chi_i^* = z_i - \frac{\mu^*}{2} \text{ for } i \in [1, s^*], \quad (16a)$$

$$\mu^* = \frac{2(\sum_{i=1}^{s^*} z_i - 1)}{s^*}, \quad (16b)$$

$$v_i^* = 0 \text{ and } v_i^* \chi_i^* = 0 \text{ for } i \in [1, s^*]. \quad (16c)$$

In addition,  $\mu^* - 2z_i$  for  $i \in [s^* + 1, n]$  are greater than or equal to zero. Therefore, we have

$$\chi_i^* = 0, v_i^* \geq 0, \text{ and } v_i^* \chi_i^* = 0 \text{ for } i \in [s^* + 1, n]. \quad (17)$$

Apparently, (16) and (17) imply (14). Besides, as  $z_i$ 's are sorted in descending order, we have

$$z_1 > \frac{\mu^*}{2}, \dots, z_{s^*} > \frac{\mu^*}{2}, z_{s^*+1} \leq \frac{\mu^*}{2}, \dots, z_n \leq \frac{\mu^*}{2}. \quad (18)$$

Algorithm 3 presents the projection without imposing the  $\ell_0$ -norm constraint. It is not difficult to know that the result of Algorithm 3 satisfies (15) to (18). As (15) to (18) imply (14), Algorithm 3 gives the solution to (12).

**2.2.2. Case 1 for optimality of Algorithm 1**

In Case 1, we consider that Algorithm 1 stops at a value  $s^*$ , such that  $z_{s^*+1} \leq \mu_{s^*}/2$  and  $s^* \leq S$ . The result is then summarized in Theorem 1.

**Theorem 1.** If Algorithm 1 terminates at a value  $s^*$ , such that  $z_{s^*+1} \leq \mu_{s^*}/2$  and  $s^* \leq S$ , then the solution  $\mathbf{x}^{s^*}$  is an optimal solution to (9), i.e., it is the solution of  $P_C(\mathbf{z})$ .

**Proof.** The proof for this case is simple. If we compare Algorithm 1 with Algorithm 3, the only difference is one of the termination conditions, i.e., “ $s = n$ ” and “ $s = S$ ”. If Algorithm 1 stops at a value  $s^*$ , such that  $z_{s^*+1} \leq \mu_{s^*}/2$  and  $s^* \leq S$ , then  $\mathbf{x}^{s^*}$  is an optimal solution of (12) with  $s^* \leq S$ . This solution is also optimal for (9). The proof is complete. ■

**2.2.3. Case 2 for optimality of Algorithm 1**

In Case 2, we consider that Algorithm 3 stops at the condition  $s = S$  and  $z_{S+1} > \mu_S/2$ . Discussion on this case is quite lengthy.

Basically, Algorithm 1 is a truncated version of Algorithm 3. Hence, studying the nature of Algorithm 3 at each iteration up to  $s = s^*$  can help us to prove the optimality of Algorithm 1, where  $s^*$  is the sparsity level of the optimal solution of (12) and  $s^* > S$ . To facilitate the discussion, let us first define some important notations:

- $\mathbf{x}^s$  is the vector obtained at the  $s$ -th iteration.

- $p(\boldsymbol{\chi}) = \|\boldsymbol{\chi} - \mathbf{z}\|_2^2$  is the objective/loss value in (9) and (12).

For Algorithm 3, at the  $s$ -th iteration, we have the following property.

**Lemma 1.** Let  $s^*$  be the sparsity level of the optimal solution of (12), where  $s^* > S$ . For Algorithm 3, at the  $s$ -th iteration,  $\mu_s/2 - z_s < 0$  holds for  $s \in [1, s^*]$ .

**Proof.** See Appendix A.

One interpretation of Algorithm 3 is that at the  $s$ -th iteration, we compute  $\mu_s$  from the first  $s$   $z_i$ 's. Afterwards, we set  $\chi_i^s$  to  $z_i - \mu_s/2$  for  $i \in [1, s]$  and remaining  $\chi_i^s$ 's to zero. Of course, when  $s = s^*$ , the projection vector  $\boldsymbol{\chi}^{s^*}$  is the optimal solution of (12).

From Lemma 1,  $\chi_i^s = z_i - \mu_s/2 > 0$  holds with  $i \in [1, s]$  and  $s \in [1, s^* - 1]$ . Hence,  $\boldsymbol{\chi}^s$  with  $s \in [1, s^* - 1]$  satisfies the nonnegativity and sum-to-one constraints in (12). However, we still cannot conclude that at the  $s$ -th iteration, setting  $\chi_i^s$  to  $z_i - \mu_s/2$  for  $i \in [1, s]$  and remaining  $\chi_i^s$ 's to zero leads to minimization of  $p(\boldsymbol{\chi}^s)$  for a given  $s$ . The following lemmas confirm the conclusion.

**Lemma 2.** For a given  $s \in [1, s^* - 1]$ , when we select the first  $s$   $\chi_i$ 's to be greater than zero, in order to minimize the loss  $p(\boldsymbol{\chi}^s)$ , we should set

$$\mu_s = \frac{2(\sum_{i=1}^s z_i - 1)}{s}, \quad (19a)$$

$$\chi_i^s = \begin{cases} z_i - \frac{\mu_s}{2}, & \text{for } i \in [1, s], \\ 0, & \text{for } i \in [s+1, n]. \end{cases} \quad (19b)$$

**Proof.** See Appendix B. Lemma 2 can be generalized to Lemma 3.

**Lemma 3.** Let  $\Theta$  be a subset of  $\{1, \dots, n\}$ , which has  $s$  elements. Define  $\mu_\Theta = 2(\sum_{j \in \Theta} z_j - 1)/s$ . Suppose that  $z_i - \mu_\Theta/2 > 0$  for  $i \in \Theta$ . If we restrict  $\chi_i > 0$  for  $i \in \Theta$  and  $\chi_i = 0$  for  $i \notin \Theta$ , then in order to minimize the loss  $p(\boldsymbol{\chi})$ , we should set

$$\chi_i^s = \begin{cases} z_i - \frac{\mu_\Theta}{2}, & \text{for } i \in \Theta, \\ 0, & \text{for } i \notin \Theta. \end{cases} \quad (20)$$

**Proof.** The proof is similar to that of Lemma 2.

Now, we start discussing how the loss  $p(\boldsymbol{\chi}^s)$  changes during Algorithm 3, and the results are summarized in Lemmas 4 and 5.

**Lemma 4.** Suppose that in Algorithm 3 we do not check  $z_{s+1} \leq \mu_s/2$  to terminate the algorithm. That is, for  $s = 1, \dots, n$ , we set

$$\mu_s = \frac{2(\sum_{j=1}^s z_j - 1)}{s}, \quad (21a)$$

$$\chi_i^s = \begin{cases} z_i - \frac{\mu_s}{2}, & \text{for } i \in [1, s], \\ 0, & \text{for } i \in [s+1, n]. \end{cases} \quad (21b)$$

Then,  $p(\boldsymbol{\chi}^s) = \|\boldsymbol{\chi} - \boldsymbol{\chi}^s\|_2^2$  is nonincreasing with respect to (w.r.t.)  $s$ . In this case,  $\boldsymbol{\chi}^s$  satisfies the sum-to-one constraint, but it may not satisfy the nonnegativity constraint.

**Proof.** See Appendix C.

**Lemma 5.** Suppose that we run Algorithm 3. That is, for  $s = 1, \dots, s^* - 1$ ,

$$\mu_s = \frac{2(\sum_{j=1}^s z_j - 1)}{s}, \quad (22)$$

$$\chi_i^s = \begin{cases} z_i - \frac{\mu_s}{2}, & \text{for } i \in [1, s], \\ 0, & \text{for } i \in [s+1, n]. \end{cases} \quad (23)$$

Then, we have  $p(\boldsymbol{\chi}^{s+1}) - p(\boldsymbol{\chi}^s) < 0$ . In this case,  $\boldsymbol{\chi}^s$  satisfies the sum-to-one and nonnegativity constraints.

**Proof.** See Appendix D.

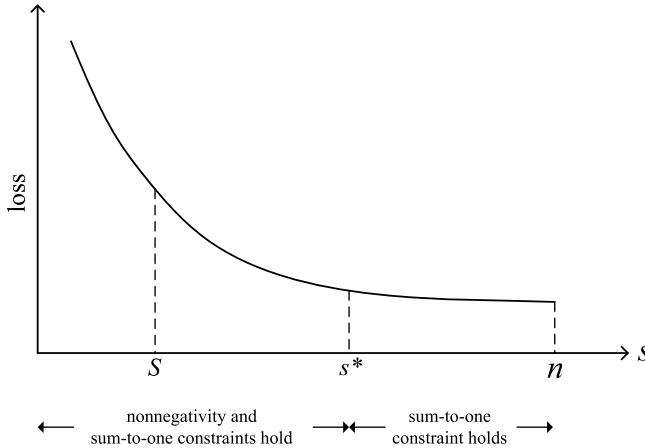


Fig. 1. Behavior of the loss in Algorithm 3.

Before we further present the proof of optimality of Algorithm 1 for stopping at  $s = S$  with  $z_{S+1} > \mu_S/2$ , we illustrate the behavior of the loss during running Algorithm 3 in Fig. 1. As shown in Fig. 1, the loss  $p(\boldsymbol{\chi}^s)$  decreases w.r.t. the sparsity  $s \in [1, s^*]$  of  $\boldsymbol{\chi}^s$  (from Lemma 5), where  $\chi_i^s > 0$  for  $i \in [1, s]$  and  $\chi_i^s > 0$  for  $i \in [1, s]$ . Note that the value of  $\boldsymbol{\chi}^s$  should be based on Lemma 2.

To complete the proof of optimality for the case that Algorithm 1 terminates at  $s = S$  and  $z_{S+1} > \mu_S/2$ , we introduce two more lemmas.

**Lemma 6.** Let  $\Theta$  be an index set  $\{1, \dots, S'\}$ , where  $S' \leq s^*$ , and let  $\boldsymbol{\chi}^{S'}$  be the solution obtained based on Lemma 2. Denote the loss as  $p(\boldsymbol{\chi}^{S'})$ . If we take out an index  $i$  from  $\Theta$  and replace it with an index  $j > S'$ . That means, we form a new index set  $\Phi = \{1, \dots, i-1, i+1, \dots, S', j\}$ . Based on  $\Phi$ , we compute  $\mu_\Phi = \frac{2(\sum_{l \in \Phi} z_l - 1)}{S}$ . If  $z_l > \mu_\Phi/2$  for  $l \in \Phi$ , then based on Lemma 3, the optimal settings of  $\boldsymbol{\chi}^\Phi$  are “ $\chi_l^\Phi = z_l^\Phi - \mu_\Phi/2$  for  $l \in \Phi$ ” and “ $\chi_l^\Phi = 0$  for  $l \in \Phi$ ”. With this  $\boldsymbol{\chi}^\Phi$ , we have  $p(\boldsymbol{\chi}^\Phi) > p(\boldsymbol{\chi}^{S'})$ .

**Proof.** See Appendix E.

**Lemma 7.** The conditions of this lemma are the same as those of Lemma 6, except that “ $z_l > \mu_\Phi/2$  for  $l \in \Phi$ ” does not hold, where  $\mu_\Phi = 2(\sum_{l \in \Phi} z_l - 1)/S$ . In order to minimize the loss for a given set  $\Phi$  with  $z_l \geq 0$  for  $l \in \Phi$ , we need to run Algorithm 3 for this  $\Phi$ . Let  $\boldsymbol{\chi}'$  be the solution, then we have  $p(\boldsymbol{\chi}') > p(\boldsymbol{\chi}^{S'})$ .

**Proof.** See Appendix F.

**Theorem 2.** If Algorithm 1 is stopped at the condition  $s = S$  and  $z_{S+1} > \mu_S/2$ , then the solution  $\boldsymbol{\chi}^S$  is an optimal solution of (9), i.e., it is solution of  $P_C(\mathbf{z})$ .

**Proof.** From Lemmas 1 to 5, the solution  $\boldsymbol{\chi}^S$  is optimal for the given index set  $\{1, \dots, S\}$ . Now, we need to show that the index set  $\{1, \dots, S\}$  is the optimal choice. From Lemmas 6 and 7, any switching on index set  $\{1, \dots, S\}$  with  $\{S+1, \dots, n\}$  leads to the increase of the loss. Therefore, the index set  $\{1, \dots, S\}$  is an optimal choice. The proof is complete. ■

### 2.3. Convergence analysis

Regarding convergence proof, the Kurdyka–Łojasiewicz properties are commonly utilized to analyze the algorithm with the sparsity regularizer [20]. Given that MIHT tackles a constrained optimization problem with  $\ell_0$ -norm, nonnegativity, and sum-to-one constraints, we adopt the majorization minimization technique [41] to establish its convergence. First, the convergence of the objective value is established in Theorem 3.

**Theorem 3.** In MIHT, the objective value  $f(\mathbf{x}) = \|\mathbf{Ax} - \mathbf{y}\|_2^2$  satisfies the following properties:

- (i)  $f(\mathbf{x})$  is lower-bounded.
- (ii) If  $\eta < 1/(2\|\mathbf{A}\|_2^2)$ ,  $f(\mathbf{x}^t) \geq f(\mathbf{x}^{t+1})$  where the equal sign holds if and only if  $\mathbf{x}^{t+1} = \mathbf{x}^t$ .

Therefore, the convergence of  $\{f(\mathbf{x}^t)\}_{t=1}^\infty$  is guaranteed with  $\eta < 1/(2\|\mathbf{A}\|_2^2)$ .

**Table 1**  
Dataset information on sparse index tracking.

Dataset	Period	Total stock	Total Day	$D_{tr}$	$D_{tst}$
Russell 2000	03/08/2015–12/12/2019	1544	1100	300	100
S&P 500	03/08/2015–12/12/2019	437	1100	300	100
NASDAQ 100	03/08/2015–12/12/2019	80	1100	300	100

**Proof.** See Appendix G.

We then analyze the convergence behavior of variable sequence  $\{\mathbf{x}^t\}_{t=1}^\infty$ .

**Theorem 4.** *With the initialization of  $\|\mathbf{x}^1\|_2^2 < +\infty$  and  $f(\mathbf{x}^1) < +\infty$ , the variable sequence  $\{\mathbf{x}^t\}_{t=1}^\infty$  generated by MIHT has the following properties:*

- (i) When  $\|\mathbf{x}\|_2 \rightarrow \infty$ ,  $h(\mathbf{x}) \rightarrow \infty$ .
- (ii)  $\mathbf{x}^t$  is bounded.
- (iii)  $\forall \epsilon > 0$ ,  $\exists T_{\max}$ , such that  $\forall t > T_{\max}$ ,  $\|\mathbf{x}^{t+1} - \mathbf{x}^t\|_2 < \epsilon$ .

In addition, we have proved that  $\{h(\mathbf{x}^t)\}_{t=1}^\infty$  converges and  $h(\mathbf{x}^{t+1}) < h(\mathbf{x}^t)$  with  $\mathbf{x}^{t+1} \neq \mathbf{x}^t$  in Theorem 3. Thereby,  $\{\mathbf{x}^t\}_{t=1}^\infty$  is guaranteed to converge.

**Proof.** See Appendix H.

#### 2.4. Computational complexity

For MIHT, the complexity of the gradient descent process is  $\mathcal{O}(mn)$ , while the complexity of the nonconvex projection is  $\mathcal{O}(n \log n + S)$ . Therefore, the total computational complexity is  $\mathcal{O}(mn + n \log n + S)$ .

In the literature, specialized linear approximation for the index tracking (SLAIT) [32] is a popular method and its complexity is  $\mathcal{O}(mn^2 + K(n^2 \log(n)))$ , where  $K$  is the number of inner iterations. Besides, the complexity of index tracking based on the adaptive elastic-net (IT-Aenet) [28] is  $\mathcal{O}(mn + n)$ . Moreover, nonnegative orthogonal matching pursuit with projected gradient descent (NNOMP-PGD) [15] has a complexity of  $\mathcal{O}(mn + Sm)$ . Although both IT-Aenet and NNOMP-PGD have low computational complexity, the former requires tuning multiple parameters to control the sparsity, whereas the latter necessitates adjusting a parameter to meet the sum-to-one constraint.

### 3. Applications and experimental results

#### 3.1. Sparse index tracking

##### 3.1.1. Problem formulation

Let  $\mathbf{y} \in \mathbb{R}^m$  be the historical collection of a market index on the past  $m$  trading days, and  $\mathbf{A} = [\mathbf{a}_1, \dots, \mathbf{a}_n] \in \mathbb{R}^{m \times n}$  be the daily returns of  $n$  assets in the past  $m$  trading days, where  $\mathbf{a}_i$  with  $i \in [1, n]$  refers to the  $i$ -th asset. In addition,  $\mathbf{x} = [x_1, \dots, x_n]^T \in \mathbb{R}^N$  denotes the weight vector, where  $x_i$  is the proportion assigned to the  $i$ -th stock. Sparse index tracking aims to replicate the market index  $\mathbf{y}$  by a few assets. Hence, it can be formulated as a linear regression optimization problem as:

$$\min_{\mathbf{x}} \|\mathbf{Ax} - \mathbf{y}\|_2^2 \quad \text{s.t. } \mathbf{x} \geq 0, \mathbf{x}^T \mathbf{1} = 1, \|\mathbf{x}\|_0 \leq S. \quad (24)$$

In the sparse index tracking, the three constraints are significant. First, the nonnegativity constraint can avoid short-selling that has the potential risk for infinite loss. While the sum-to-one implies that  $x_n$  is an accurate proportion and thus fund managers can allocate the capital according to  $\mathbf{x}$ . For the sparsity constraint, it is the number of selected assets.

##### 3.1.2. Experimental setting

Four algorithms, namely, SLAIT, accelerated SLAIT (ASLAIT) [32] and IT-Aenet [28], NNOMP-PGD [15], are adopted to compare with the proposed MIHT. Note that in the SLAIT, IT-Agent and ASLAIT, we cannot explicitly control the number of selected stocks. We consider three real-world datasets, viz. Russell 2000, S&P 500 and NASDAQ 100. Since the selected duration is long, not all stocks can cover the whole period, resulting in excluding some assets according to the common practice [42,43]. Therefore, the adopted Russell 2000, S&P 500 and NASDAQ 100 consist of 1544, 437 and 80 stocks, respectively. Table 1 tabulates the details of each dataset, that is, time period of dataset, total days  $D$ , training days  $D_{tr}$ , and test days  $D_{tst}$ .

A moving window strategy is used to assess all algorithms. Compared with the scheme that utilizes the whole data to test, it has two advantages. First, more data can be used as the test set. Besides, it can lessen the effect on the result from data characteristics, namely, stable, recessionary and bubbly markets. Hence, we can attain a more reliable generalization error. The first window is from

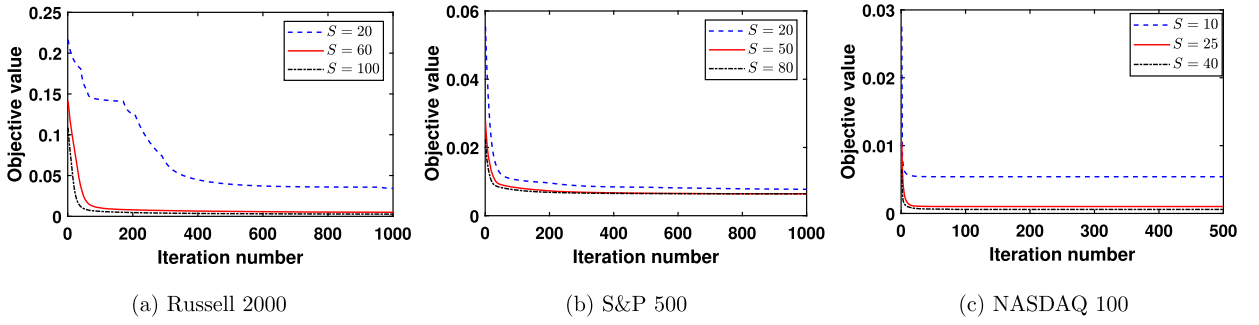


Fig. 2. Objective function value versus iteration number on financial datasets.

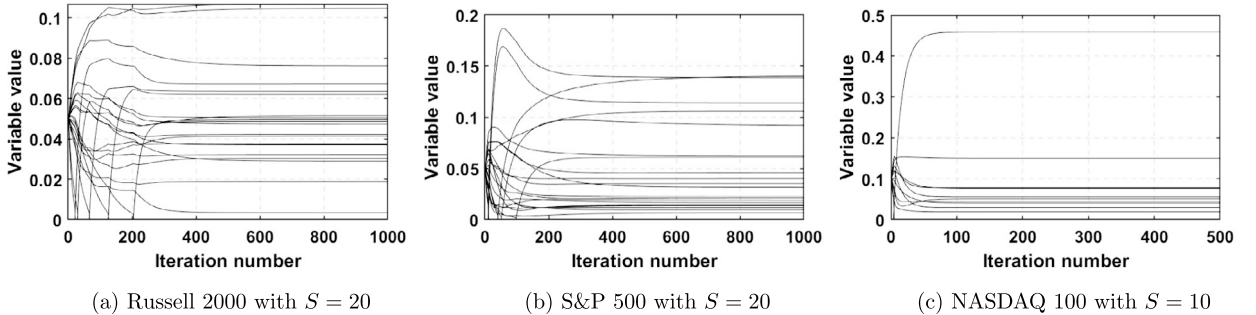


Fig. 3. Sequence value versus iteration number on financial dataset.

the 1st day covering  $D_{\text{tr}} + D_{\text{tst}}$  days, in which first  $D_{\text{tr}}$  days are adopted as a training set and then the remaining  $D_{\text{tst}}$  days are considered as a test set. Then, we move the window forward  $D_{\text{tst}}$  days and attain the second window. Note that the second window should have a  $D_{\text{tr}}$ -day overlapping with the first window. Similar to the first window, the second window allocates first  $D_{\text{tr}}$  days and the following  $D_{\text{tst}}$  days to the training and test sets, respectively. Furthermore, the window continues to move forward until we consume the whole data.

### 3.1.3. Performance metric

The magnitude of the daily tracking error (MDTE) [32] is adopted to evaluate recovery performance, defined as:

$$\text{MDTE} = \frac{1}{D - D_{\text{tr}}} \|\text{diag}(\tilde{\mathbf{A}}\tilde{\mathbf{X}}) - \tilde{\mathbf{y}}\|_2, \quad (25)$$

where  $\tilde{\mathbf{A}} \in \mathbb{R}^{(D-D_{\text{tr}}) \times n}$ ,  $\tilde{\mathbf{X}} \in \mathbb{R}^{n \times (D-D_{\text{tr}})}$  and  $\tilde{\mathbf{y}} \in \mathbb{R}^{D-D_{\text{tr}}}$ . It is easy to know that  $\tilde{\mathbf{A}}$  and  $\tilde{\mathbf{y}}$  consist of all testing data. While one recovered  $\mathbf{x}$  constructs a matrix  $\tilde{\mathbf{X}} \in \mathbb{R}^{n \times D_{\text{tst}}}$  whose all columns are equal to  $\mathbf{x}$ . Hence,  $\tilde{\mathbf{X}}$  is comprised of all  $\tilde{\mathbf{X}}$ . The MDTE is presented in basis points (bps), where 1 bps is equivalent to  $10^{-4}$ .

### 3.1.4. Convergence

Prior to presenting the numerical results, empirical convergence of the MIHT algorithm is evaluated. Since our objective function differs from the existing ones, it is not reasonable to compare the objective values of different algorithms. Consequently, we solely analyze the convergence behavior of our method.

Fig. 2 shows the objective value versus iteration number on three financial datasets. We see that the objective value decreases as the number of iterations increases. Besides, a larger  $S$  results in a smaller objective value. Fig. 3 illustrates the dynamics of sequence value. We observe that the proposed algorithm is able to achieve a convergent sequence.

### 3.1.5. Experimental results

Figs. 4 (a), (b), and (c) show the prediction error of four algorithms on Russell 2000, S&P 500 and NASDAQ 100 datasets, respectively. It is seen that the MIHT demonstrates obvious superiority over SLAIT, ASLAIT and NNOMP-PGD on Russell 2000, S&P 500 and NASDAQ 100, especially in small sparsity levels. In high sparsity levels, the SLAIT and NNOMP-PGD have comparable performance with our algorithm, but the MIHT is still superior to the competing methods. Note that in the SLAIT and ASLAIT, it is quite time consuming to tune their penalty parameters in order to attain the desired sparsity level. On the other hand, in the MIHT, we can directly control the sparsity via setting  $S$ .

For IT-Aenet, its sparsity is affected by three penalty parameters and hence it is difficult to tune parameters to attain the same sparsity among all windows. Thereby, we set a group of parameters and test the IT-Aenet on all windows, resulting in different sparsity

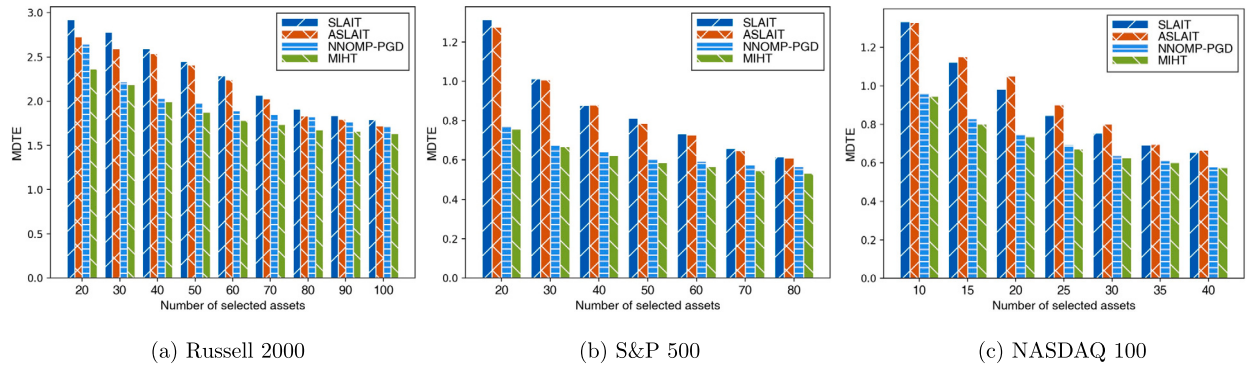


Fig. 4. Prediction error of different algorithms.

**Table 2**  
Prediction error of MIHT and IT-Aenet on different datasets.

Dataset	Method	Window 1	Window 2	Window 3	Window 4	Window 5	Window 6	Window 7	Window 8
Russell 2000	Sparsity	65	63	57	60	37	33	76	132
	our MIHT	<b>5.66</b>	<b>4.48</b>	<b>4.65</b>	<b>5.87</b>	<b>5.59</b>	<b>9.01</b>	<b>5.28</b>	<b>5.04</b>
	IT-Aenet	9.22	7.33	6.66	9.80	6.68	13.63	9.09	8.74
S&P 500	Sparsity	39	61	100	19	63	63	59	58
	our MIHT	<b>2.73</b>	<b>1.38</b>	<b>1.37</b>	<b>4.18</b>	<b>1.47</b>	<b>2.07</b>	<b>1.66</b>	<b>1.86</b>
	IT-Aenet	5.49	3.83	2.48	7.39	6.39	10.11	3.40	6.18
NASDAQ 100	Sparsity	43	43	43	41	42	41	44	42
	our MIHT	2.32	<b>1.63</b>	<b>1.85</b>	<b>1.80</b>	<b>1.47</b>	<b>1.87</b>	<b>1.41</b>	<b>1.73</b>
	IT-Aenet	<b>2.12</b>	2.04	2.95	2.85	2.61	2.87	2.39	2.36

on different windows. Then, we control  $S$  to make the MIHT having the same sparsity as the IT-Aenet in each window. Table 2 lists the results of the MIHT and IT-Aenet. It is seen that the MIHT obtains lower MDTEs than the IT-Aenet except for the first window on NASDAQ 100.

### 3.2. Hyperspectral unmixing

#### 3.2.1. Problem formulation

Consider that  $\mathbf{Y} \in \mathbb{R}^{m \times p}$  is the observed hyperspectral image with  $m$  bands and  $p$  pixels. In practice, the acquired hyperspectral image is a 3rd-order tensor, involving  $m$  matrices. The matrices are vectorized and arranged as  $\mathbf{Y}$ . Besides, let  $\mathbf{A} \in \mathbb{R}^{m \times n}$  denote a spectral library having  $n$  spectral signatures. Hyperspectral unmixing is to seek a linear combination of endmembers for  $\mathbf{Y}$  from the spectral library  $\mathbf{A}$ , formulated as:

$$\mathbf{Y} = \mathbf{AX} + \mathbf{N} \quad (26)$$

where  $\mathbf{X} \in \mathbb{R}^{n \times p}$  is the fractional abundance matrix, and  $\mathbf{N} \in \mathbb{R}^{L \times N}$  is the noise matrix. In practice, the fractional abundance matrix  $\mathbf{X}$  is also subject to the nonnegativity, sum-to-one and sparsity constraints. Since each entry denotes the weight of spectral signature in a pixel,  $\mathbf{X}$  is nonnegative. The sum-to-one property indicates that abundances give the fractional proportions, or percentages, of the different spectral signatures in a pixel. Moreover, a pixel is likely to be sensitive for a few of the spectral signatures and hence the column of  $\mathbf{X}$  is sparse, resulting in a sparse  $\mathbf{X}$ . Therefore, the hyperspectral unmixing problem can be formulated as

$$\min_{\mathbf{X}} \|\mathbf{AX} - \mathbf{Y}\|_F^2, \text{ s.t. } \mathbf{X} \geq 0, \mathbf{1}^T \mathbf{X} = \mathbf{1}^T, \mathbf{X} \text{ is sparse.} \quad (27)$$

As each column of  $\mathbf{X}$  is independent, (27) can be decomposed into  $p$  vector optimization problems

$$\min_{\mathbf{x}_j} \|\mathbf{Ax}_j - \mathbf{y}_j\|_2^2 \text{ s.t. } \mathbf{x}_j \geq 0, \mathbf{1}^T \mathbf{x}_j = 1, \|\mathbf{x}_j\|_0 \leq S \quad (28)$$

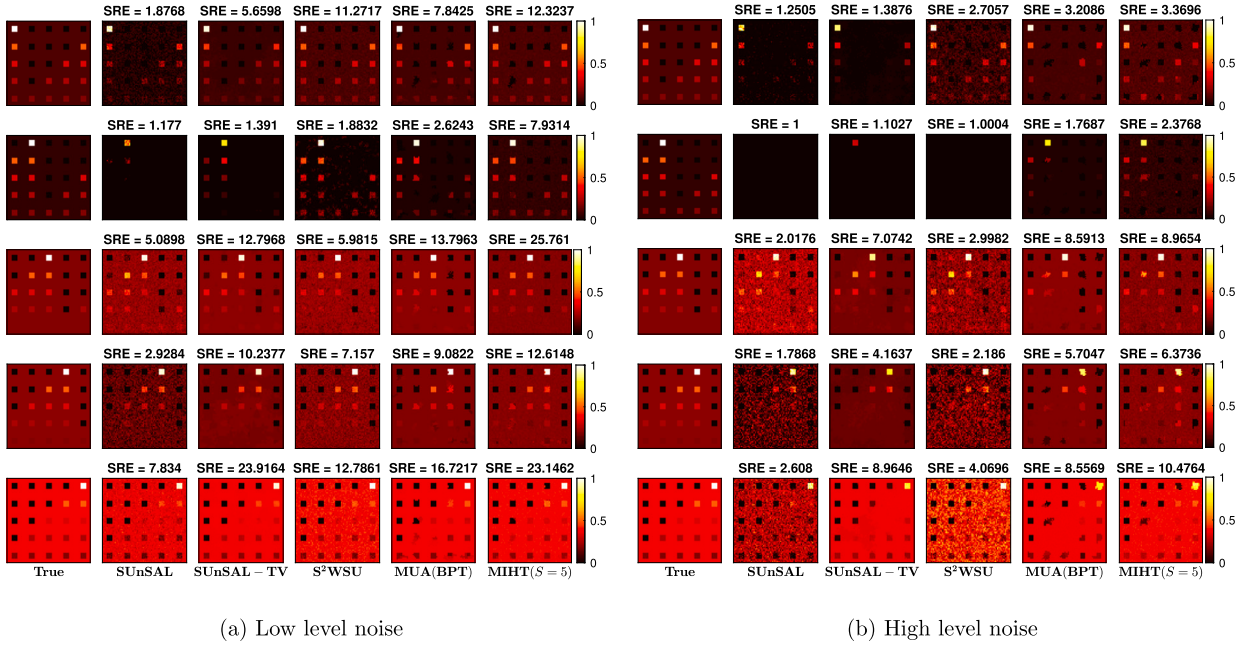
where  $\mathbf{x}_j$  and  $\mathbf{y}_j$  are the  $j$ -th columns of  $\mathbf{X}$  and  $\mathbf{Y}$ , respectively. Thereby, the MIHT can be utilized to handle the hyperspectral unmixing problem.

#### 3.2.2. Experimental setting

The MIHT is compared with four algorithms, namely, sparse unmixing by variable splitting and augmented Lagrangian (SUnSAL) [44], total variation SUnSAL (SUnSAL-TV) [25], spectral-spatial weighted sparse unmixing ( $S^2$ WSU) [26] and multiscale sparse unmixing algorithm with binary partition tree based segmentation (MUA (BPT)) [45].

**Table 3**  
Dataset information on hyperspectral unmixing.

Dataset	Image dimensions	Band number
DC1	$75 \times 75$	224
DC2	$100 \times 100$	224
Samson	$95 \times 95$	156
Jasper Ridge	$100 \times 100$	198



(a) Low level noise

(b) High level noise

**Fig. 5.** Original and reconstructed abundance maps by different algorithms for DC1 in white Gaussian noise.

We test with four open datasets, namely, synthetic data cube 1 (DC1), synthetic data cube 2 (DC2), real-world Samson and Jasper ridge.<sup>1</sup> Table 3 tabulates the details of the four datasets, including bands and image dimensions. DC1 and DC2 possess 5 and 9 endmembers, respectively, selected from a synthetic library  $\mathbf{A}_1 \in \mathbb{R}^{224 \times 240}$  that is generated by a subset of 240 materials from U.S. Geological Survey (USGS) library.<sup>2</sup> Besides, the abundance map of DC1 consists of 25 squares that are uniformly distributed over a background in five rows and columns. While, for DC2, its abundance maps are constructed by a Dirichlet distribution with the center of a Gaussian random field. Moreover, white Gaussian noise is added to the DC1 and DC2 data for generating  $\mathbf{Y}$ . The performance of reconstruction is evaluated by the signal-to-reconstruction error (SRE) [25]:

$$\text{SRE} = 10 \log_{10} \left( \frac{\|\tilde{\mathbf{X}}\|_F^2}{\|\tilde{\mathbf{X}} - \mathbf{X}\|_F^2} \right), \quad (29)$$

where  $\tilde{\mathbf{X}}$  is the ground truth. It is worth pointing out that a large SRE indicates high estimation accuracy.

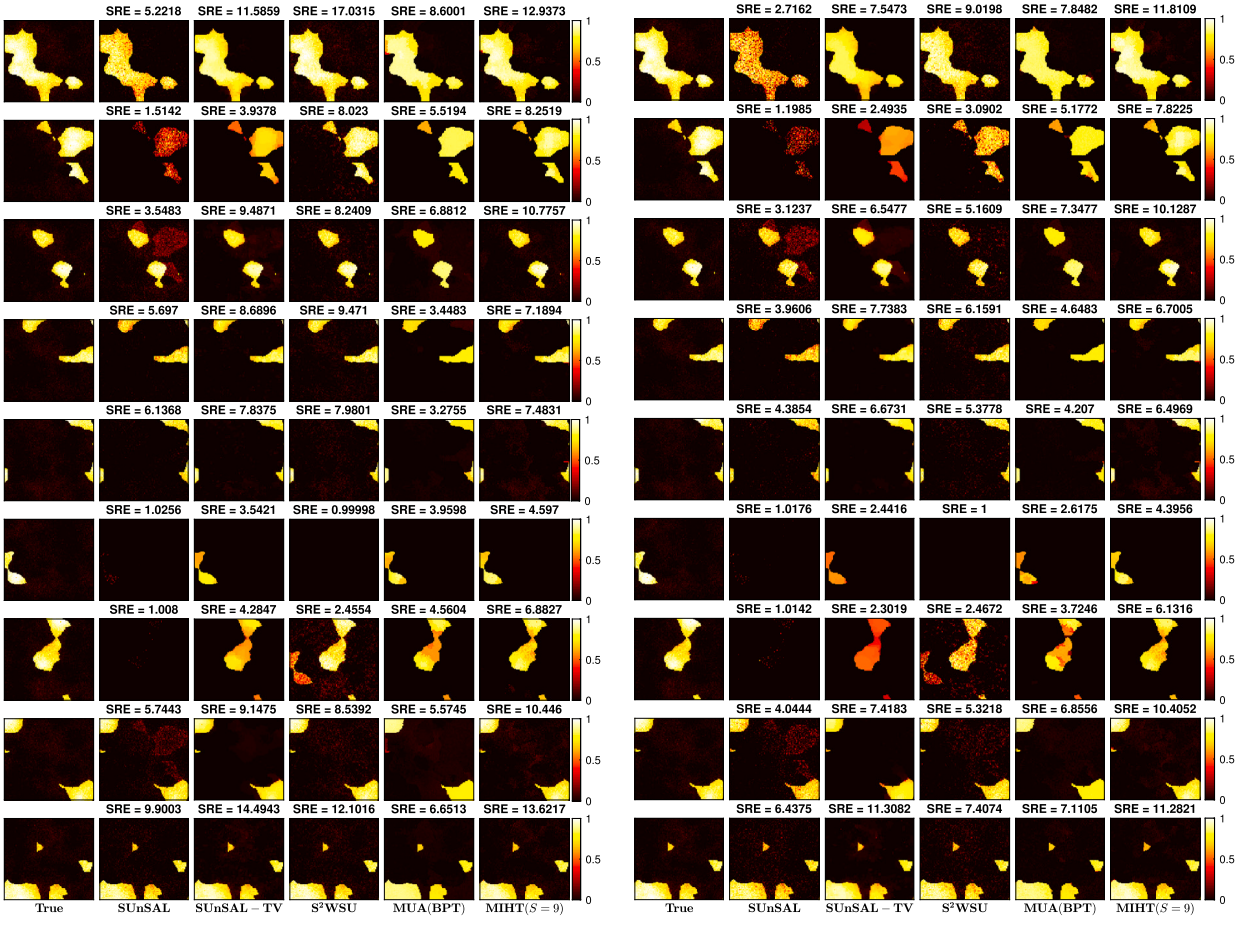
For Samson and Jasper ridge, their spectral libraries are constructed by the image-based library construction method [46] based on the captured hyperspectral images. Hence, the dimensions of spectral libraries are  $156 \times 105$  for Samson and  $198 \times 529$  for Jasper ridge. Moreover, the color composite image and ground truth are illustrated in Figs. 7 and 8 that can be utilized to evaluate the performance of different algorithms.

### 3.2.3. Experimental results

Figs. 5 (a) and (b) plot the reconstructed abundance maps for DC1 in the white Gaussian noise with  $\sigma = 0.0242$  and  $\sigma = 0.0764$ , respectively. The corresponding SREs are shown at the top of the images. It is seen from Fig. 5 (a) that the MIHT algorithm has the largest SREs on endmembers 1, 2, 3, and 4. For the fifth endmember, the SRE of our method is slightly smaller than that of SUNSAL-TV, but is much larger than those of other three approaches. In the high level noise, our MIHT has the largest SREs on all endmembers

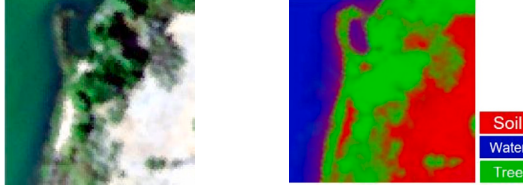
<sup>1</sup> <https://rslab.ut.ac.ir>.

<sup>2</sup> <https://www.usgs.gov/human-capital/usgs-library>.



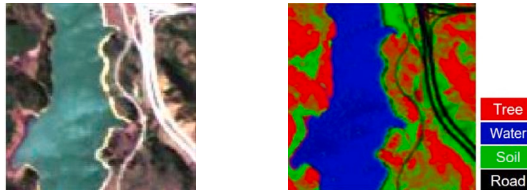
(a) Low level noise

(b) High level noise

**Fig. 6.** Original and reconstructed abundance maps by different algorithms for DC2 in white Gaussian noise.

(a) Color composite image

(b) Ground truth

**Fig. 7.** Illustration of Samson dataset.

(a) Color composite image

(b) Ground truth

**Fig. 8.** Illustration of Jasper dataset.

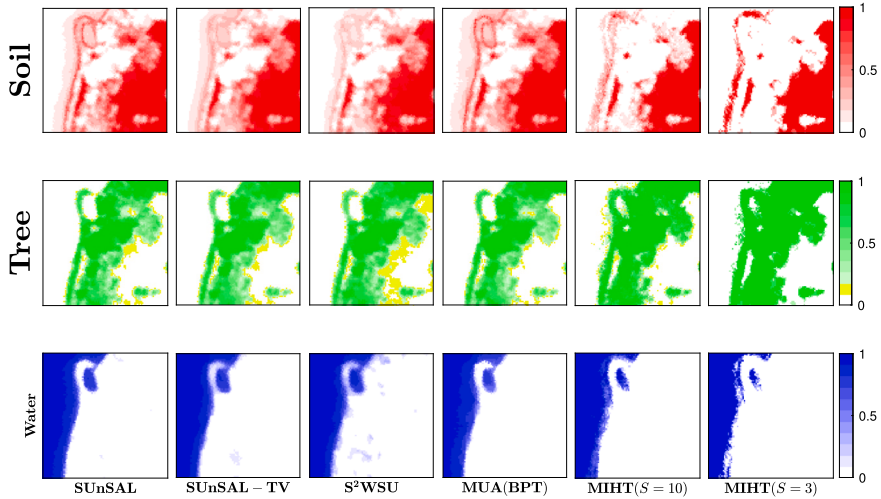


**Fig. 9.** Reconstructed abundance maps by different algorithms for Samson hyperspectral image.

among the five methods. For the reconstructed abundance maps of DC2, they are depicted in Figs. 6 (a) and (b). We see from the low level noise case that our approach attains maximum SREs on endmembers 2, 3, 6, 7 and 8. In the presence of strong intensity noise, our MIHT obtains the largest SREs on endmembers 1, 2, 3, 6, 7 and 8. Hence, the MIHT is superior to SUNSAL, SUNSAL-TV,  $S^2$ WSU and MUA (BPT).

The reconstructed abundance maps for Samson dataset are plotted in Fig. 9. It is seen that the predicted value of the MIHT is closer to 1 in the water abundance map. Since it is a classification problem, our algorithm is more accurate than SUNSAL, SUNSAL-TV,  $S^2$ WSU and MUA (BPT).

Besides, the tree in the bottom right corner is recognized by all approaches, while the results from our MIHT are more reliable due to a large value. For the soil abundance map, our algorithm attains a clearer result, that is, obvious boundaries. This is because the proposed method can accurately control the sparsity of each column, that is, the number of effective spectral signatures of each pixel. While SUNSAL, SUNSAL-TV,  $S^2$ WSU and MUA (BPT) achieve an approximate sparsity for all pixels via tuning the penalty parameter. Hence, some pixels may have a large or small sparsity.

The reconstructed abundance maps of Jasper ridge are shown in Fig. 10. From the ground truth, we know that there is no road to the left of river. However, SUNSAL, SUNSAL-TV, and MUA (BPT) describe a continuous outline of it. The result with  $s = 6$  computed by our method do not provide this wrong information. Besides, our MIHT provides more reliable information (the value close to 1) on soil to the right of river. Moreover, our MIHT with a small sparsity offers more information on the tree, such as the bright area to the left of river.

#### 4. Conclusion

In this paper, we have derived the MIHT to handle the linear regression problem subject to sparsity, nonnegativity and sum-to-one constraints. The proposed algorithm consists of two steps, namely, gradient descent and nonconvex projection. Compared with the algorithms in the literature, the key novelty is that the MIHT is able to explicitly and accurately control the sparsity via setting a parameter. Moreover, the solution computed by the MIHT satisfies the sum-to-one constraint, hence it does not require normalization for the solution. Experimental results on sparse index tracking and hyperspectral unmixing demonstrate that our MIHT is superior to SLAIT, ASLAIT, IT-Aenet, NNOMP-PGD, SUNSAL, SUNSAL-TV,  $S^2$ WSU and MUA (BPT).

Given that our optimization problem utilizes  $\ell_2$ -norm (or Frobenius norm) as the loss function, it is assumed that data do not contain anomalies. In practical scenarios, stock prices may experience a sudden slump followed by a rapid recovery. Besides, hyperspectral data may be corrupted by impulsive noise. However, the  $\ell_2$ -norm cannot achieve reliable performance in such scenarios. If we intend to process the data with anomalies, we require adopting  $\ell_p$ -norm ( $0 < p < 2$ ) or M-estimator, such as Huber loss as the objective function. Conversely, these robust loss functions cannot attain the optimal performance in Gaussian noise scenarios. Therefore, one of our future works is to design an adaptive loss function or algorithm that can effectively handle mixed situations. Additionally, we plan to explore further applications of MIHT. For instance, in processing underwater acoustic signals or telemonitoring diaphragmatic electromyogram signals [34,35], the domain transformation matrix can be designed in a way that the sparse signal exhibits sum-to-one and nonnegativity properties.

#### Funding statements

The work described in this paper was supported in part by the Young Innovative Talents Project of Guangdong Provincial Department of Education (Natural Science) under Grant 2023KQNCX063, in part by a grant from City University of Hong Kong (Project No.

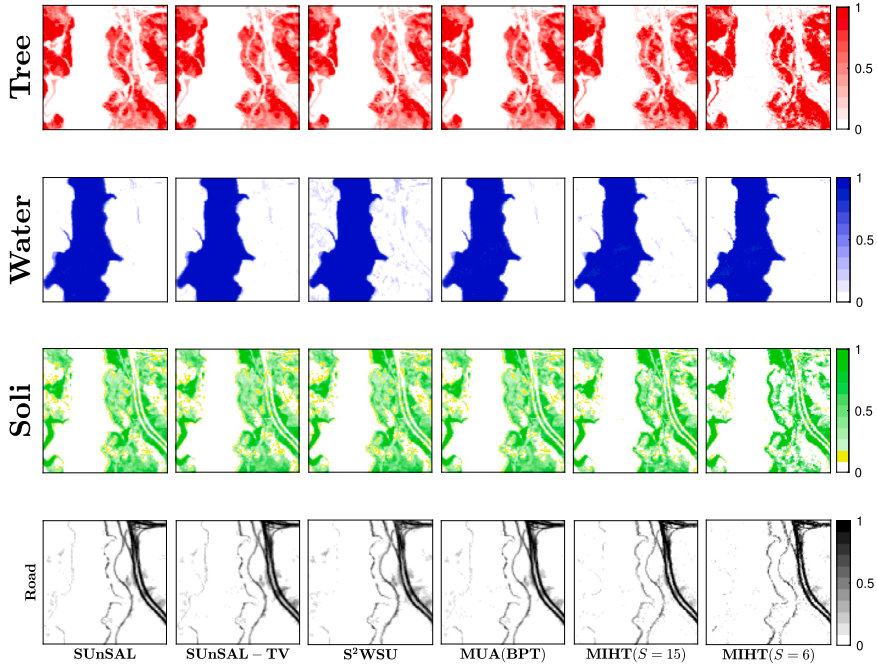


**Fig. 10.** Reconstructed abundance maps by different algorithms for Jasper hyperspectral image.

CityU 11207922), in part by a grant from City University of Hong Kong (Project No. 7006084), in part by the Guangdong Basic and Applied Basic Research Foundation 2021A1515011706.

#### CRediT authorship contribution statement

**Xiao-Peng Li:** Writing – review & editing, Writing – original draft, Validation, Software, Formal analysis, Data curation. **Chi-Sing Leung:** Writing – review & editing, Validation, Supervision, Project administration. **Hing Cheung So:** Writing – review & editing, Writing – original draft, Supervision, Formal analysis.

#### Declaration of competing interest

The authors declare the following financial interests/personal relationships which may be considered as potential competing interests: Xiaopeng Li has patent METHOD AND ANALYSIS DEVICE FOR TRACKING MARKET INDEX AND UNMIXING HYPERSPECTRAL IMAGE USING MODIFIED ITERATIVE HARD THRESHOLDING FOR NONNEGATIVE SPARSE RECOVERY UNDER SUM-TO-ONE pending to US 17/575,652.

#### Data availability

Data will be made available on request.

#### Appendix A. Proof of Lemma 1

As mentioned at the end of Section IV.A.1, Algorithm 3 leads to an optimal solution of (12). When Algorithm 3 stops at  $s^*$ , we have

$$\frac{\mu_{s^*}}{2} - z_{s^*} < 0. \quad (\text{A.1})$$

Besides, from the definition of  $\mu_s$ , we have

$$\mu_{s^*} = \frac{2(\sum_{i=1}^{s^*} z_i - 1)}{s^*} = \frac{2(\sum_{i=1}^s z_i - 1) + 2\sum_{i=s+1}^{s^*} z_i}{s^*} = \frac{s\mu_s + 2\sum_{i=s+1}^{s^*} z_i}{s^*}. \quad (\text{A.2})$$

Plugging (A.2) into (A.1) yields:

$$s\mu_s + 2 \sum_{i=s+1}^{s^*} z_i - 2s^*z_{s^*} < 0$$

$$\Leftrightarrow s\mu_s - 2sz_{s^*} + 2 \sum_{i=s+1}^{s^*} (z_i - z_{s^*}) < 0. \quad (\text{A.3})$$

It is known that  $z_i \geq z_{s^*}$  with  $1 \leq i < s^*$ . Thus,

$$\sum_{i=s+1}^{s^*} (z_i - z_{s^*}) \geq 0, \quad (\text{A.4})$$

and then

$$s\mu_s - 2sz_{s^*} < 0 \Leftrightarrow \frac{\mu_s}{2} - z_{s^*} < 0 \Rightarrow \frac{\mu_s}{2} - z_s < 0. \quad (\text{A.5})$$

The proof is complete. ■

## Appendix B. Proof of Lemma 2

Assume that

$$\chi_i^s = \begin{cases} z_i - \frac{a_i}{2} > 0, & \text{for } i \in [1, s], \\ 0, & \text{for } i \in [s+1, n]. \end{cases} \quad (\text{B.1})$$

It is required that  $\sum_{i=1}^s \chi_i^s = 1$ , resulting in

$$\sum_{i=1}^s a_i = 2 \left( \sum_{i=1}^s z_i - 1 \right). \quad (\text{B.2})$$

With (B.1), to minimize the loss  $p(\boldsymbol{\chi}^s)$  subject to the sum-to-one constraint, we need to solve the following problem:

$$\min_{a_i} \frac{1}{4} \sum_{i=1}^s a_i^2 + \sum_{i=s+1}^n z_i^2, \text{ s.t. } \sum_{i=1}^s a_i = 2 \left( \sum_{i=1}^s z_i - 1 \right). \quad (\text{B.3})$$

It is not difficult to show that the solution for (B.3) is

$$a_i = \frac{2(\sum_{j=1}^s z_j - 1)}{s} \text{ for } i = 1, \dots, s. \quad (\text{B.4})$$

With (B.4), we obtain (19) and the proof is complete. ■

## Appendix C. Proof of Lemma 4

$$\begin{aligned} p(\boldsymbol{\chi}^{s+1}) - p(\boldsymbol{\chi}^s) &= \|\mathbf{z} - \boldsymbol{\chi}^{s+1}\|_2^2 - \|\mathbf{z} - \boldsymbol{\chi}^s\|_2^2 \\ &= \sum_{i=1}^n (z_i - \chi_i^{s+1})^2 - \sum_{i=1}^n (z_i - \chi_i^s)^2 \\ &= \sum_{i=1}^{s+1} \frac{\mu_{s+1}^2}{4} - \left( \sum_{i=1}^s \frac{\mu_s^2}{4} + z_{s+1}^2 \right) \\ &= \frac{1}{4} ((s+1)\mu_{s+1}^2 - s\mu_s^2 - 4z_{s+1}^2). \end{aligned} \quad (\text{C.1})$$

According to (21), we have

$$\mu_{s+1} = \frac{2(\sum_{i=1}^{s+1} z_i - 1)}{s+1} \text{ and } \mu_s = \frac{2(\sum_{i=1}^s z_i - 1)}{s}. \quad (\text{C.2})$$

Thereby, the relationship among  $\mu_s$ ,  $\mu_{s+1}$  and  $z_{s+1}$  is

$$\begin{aligned} (s+1)\mu_{s+1} - 2 \sum_{i=1}^{s+1} z_i &= s\mu_s - 2 \sum_{i=1}^s z_i \\ \Rightarrow (s+1)\mu_{s+1} - s\mu_s &= 2z_{s+1} \\ \Rightarrow (s+1)^2 \mu_{s+1}^2 + s^2 \mu_s^2 - 2s(s+1)\mu_{s+1}\mu_s &= 4z_{s+1}^2 \end{aligned} \quad (\text{C.3})$$

Then, substituting (C.3) into (C.1) yields

$$\begin{aligned}
& p(\boldsymbol{\chi}^{s+1}) - p(\boldsymbol{\chi}^s) \\
&= \frac{1}{4}((s+1)\mu_{s+1}^2 - s\mu_s^2 - (s+1)^2\mu_{s+1}^2 - s^2\mu_s^2 \\
&\quad + 2s(s+1)\mu_{s+1}\mu_s) \\
&= \frac{1}{4}(-s(s+1)\mu_{s+1}^2 - s(s+1)\mu_s^2 + 2s(s+1)\mu_{s+1}\mu_s) \\
&= -\frac{1}{4}s(s+1)(\mu_{s+1}^2 + \mu_s^2 - 2\mu_{s+1}\mu_s) \\
&= -\frac{1}{4}s(s+1)(\mu_{s+1} - \mu_s)^2 \leq 0.
\end{aligned} \tag{C.4}$$

The proof is complete. ■

#### Appendix D. Proof of Lemma 5

Since we run Algorithm 3, for  $s = 1, \dots, s^* - 1$ , we have  $\mu_s/2 - z_{s+1} < 0$ . From Lemma 4,  $p(\boldsymbol{\chi}^{s+1}) - p(\boldsymbol{\chi}^s) < 0$  can be proved when  $\mu_{k+1} \neq \mu_k$ .

If " $\mu_{s+1} = \mu_s$ " is true, then

$$\begin{aligned}
\mu_{s+1} = \mu_s &\Leftrightarrow \frac{\sum_{i=1}^{s+1} z_i - 1}{s+1} = \frac{\sum_{i=1}^s z_i - 1}{s} \\
\Leftrightarrow \frac{\sum_{i=1}^s z_i - 1 + z_{s+1}}{s+1} &= \frac{\sum_{i=1}^s z_i - 1}{s} \\
\Leftrightarrow z_{s+1} &= \frac{\sum_{i=1}^s z_i - 1}{s} \Leftrightarrow \frac{\mu_s}{2} - z_{s+1} = 0.
\end{aligned} \tag{D.1}$$

Now, we have contradiction. Thereby, when  $s \in [1, s^* - 1]$ , we have  $\mu_{s+1} \neq \mu_s$ , as well as  $p(\boldsymbol{\chi}^{s+1}) - p(\boldsymbol{\chi}^s) < 0$ . The proof is complete. ■

#### Appendix E. Proof of Lemma 6

$$\begin{aligned}
& p(\boldsymbol{\chi}^{S'}) - p(\boldsymbol{\chi}^\Phi) \\
&= S \left( \frac{\sum_{l'=1, l' \neq i}^n z_{l'} + z_i - 1}{S'} \right)^2 + z_j^2 + \sum_{l'=S'+1, l' \neq j}^n z_{l'}^2 \\
&\quad - S \left( \frac{\sum_{l'=1, l' \neq i}^n z_{l'} + z_j - 1}{S'} \right)^2 - z_i^2 - \sum_{l'=S'+1, l' \neq j}^n z_{l'}^2 \\
&= \frac{(z_j - z_i)[(S' - 1)(z_j + z_i) - 2(\sum_{l'=1, l' \neq i}^n z_{l'} - 1)]}{S'}.
\end{aligned} \tag{E.1}$$

Since  $z_l > \mu_\Theta/2$  for  $l \in \Theta$  and  $z_l > \mu_\Phi/2$  for  $l \in \Phi$ , we have

$$(S' - 1)z_i > \sum_{l'=1, l' \neq i}^{S'} z_{l'} - 1 \text{ and } (S' - 1)z_j > \sum_{l'=1, l' \neq i}^{S'} z_{l'} - 1. \tag{E.2}$$

Moreover,  $z_j < z_i$ . Therefore, (E.1) implies  $p(\boldsymbol{\chi}^{S'}) - p(\boldsymbol{\chi}^\Phi) < 0$ . Fig. E.11 is a graphical illustration of this case. The proof is complete. ■

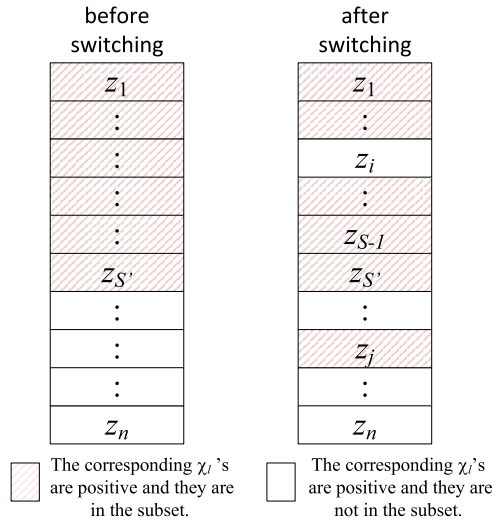
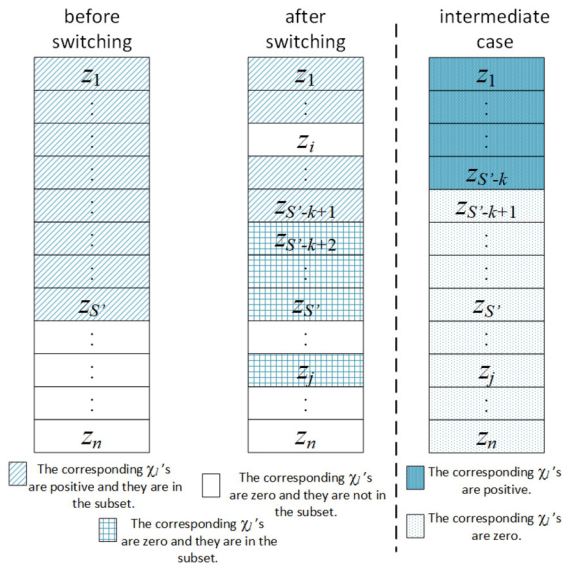
#### Appendix F. Proof of Lemma 7

Solution  $\boldsymbol{\chi}'$  corresponds to two cases, shown in Figs. F.12 and F.13. Let  $S' - k$  be the sparsity of  $\boldsymbol{\chi}'$ , where  $k \geq 1$ . Note that we do not know the exact sparsity of  $\boldsymbol{\chi}'$  but it must be less than  $S'$  according to the given conditions.

In the first case, shown in Fig. F.12,  $i$  is less than  $S' - k + 1$ . The loss  $p(\boldsymbol{\chi}')$  of  $\boldsymbol{\chi}'$  is greater than that of the intermediate case according Lemma 6. In addition, according to Lemma 2, the loss of the intermediate case is greater than  $p(\boldsymbol{\chi}^{S'})$ .

In the second case, shown in Fig. F.13,  $i$  is less than  $S' - k + 1$ . The loss  $p(\boldsymbol{\chi}')$  of  $\boldsymbol{\chi}'$  is equal to that of the intermediate case according Lemma 6. In addition, according to Lemma 2, the loss of the intermediate case is greater than  $p(\boldsymbol{\chi}^{S'})$ .

To sum up, for both cases, we have  $p(\boldsymbol{\chi}') > p(\boldsymbol{\chi}^{S'})$ . The proof is complete. ■

Fig. E.11. Illustration of switching, where  $z_i$  is greater than  $\mu_0/2 \forall i \in \Theta$ .Fig. F.12. Illustration of switching, where after switching we need to set  $k$   $x_j$ 's to zero and the switching out index  $i$  is less than  $z_{S-k+1}$ .

## Appendix G. Proof of Theorem 3

Property (i) is easy to be verified since  $f(\mathbf{x})$  is minimized by the  $\ell_2$ -norm.

We then introduce a surrogate function to facilitate proving Property (ii). The surrogate function is defined as

$$\varepsilon(\mathbf{x}, \tilde{\mathbf{x}}) = \|\mathbf{A}\mathbf{x} - \mathbf{y}\|_2^2 - \|\mathbf{A}\mathbf{x} - \mathbf{A}\tilde{\mathbf{x}}\|_2^2 + \frac{1}{2\eta} \|\mathbf{x} - \tilde{\mathbf{x}}\|_2^2 + I(\mathbf{x}), \quad (\text{G.1})$$

where  $I(\mathbf{x})$  is an indicator function:

$$I(\mathbf{x}) = \begin{cases} 0, & \text{for } \mathbf{x} \in C, \\ +\infty, & \text{otherwise.} \end{cases} \quad (\text{G.2})$$

With  $\tilde{\mathbf{x}} = \mathbf{x}'$ , the surrogate function is rewritten as

$$\varepsilon(\mathbf{x}, \mathbf{x}') = \frac{1}{2\eta} \|\mathbf{x} - (\mathbf{x}' - 2\eta \mathbf{A}^\top (\mathbf{A}\mathbf{x}' - \mathbf{y}))\|_2^2 + I(\mathbf{x}) + c, \quad (\text{G.3})$$

where  $c = \frac{1}{2\eta} (\|\mathbf{x}'\|_2^2 - \|\mathbf{x}' - 2\eta \mathbf{A}^\top (\mathbf{A}\mathbf{x}' - \mathbf{y})\|_2^2) + \|\mathbf{y}\|_2^2 - \|\mathbf{A}\mathbf{x}'\|_2^2$ . Given  $\mathbf{x}'$ , optimizing the surrogate function is equivalent to

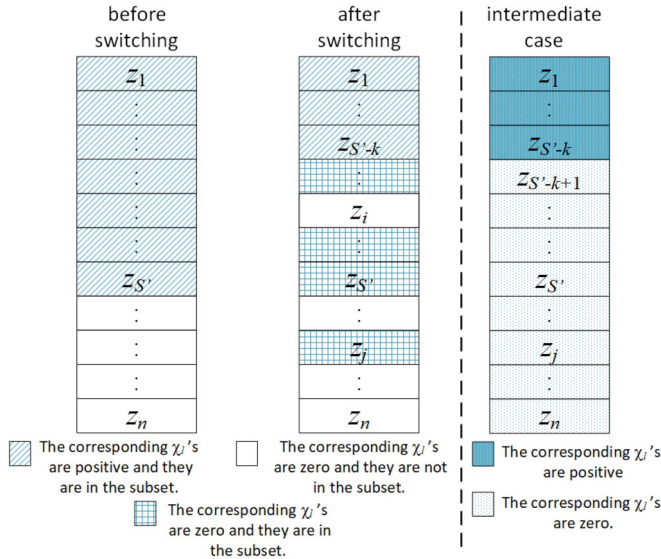


**Fig. F.13.** Illustration of switching, where after switching we need to set  $k$   $x_i$ 's to zero and the switching out index  $i$  is not less than  $z_{S'-k+1}$ .

$$\begin{aligned} \min_{\mathbf{x}} \varepsilon(\mathbf{x}, \mathbf{x}') &= \min_{\mathbf{x}} \frac{1}{2\eta} \|\mathbf{x} - \mathbf{z}'\|_2^2 \\ \text{s.t. } \mathbf{z}' &= \mathbf{x}' - 2\eta \mathbf{A}^T (\mathbf{Ax}' - \mathbf{y}), \\ \mathbf{x} &\in \mathcal{C}. \end{aligned} \quad (\text{G.4})$$

It is clear that one minimizer is obtained using our projection operator:

$$\mathbf{x}'^{t+1} = P_C \left( \mathbf{x}' - 2\eta \mathbf{A}^T (\mathbf{Ax}' - \mathbf{y}) \right). \quad (\text{G.5})$$

That is, given  $\mathbf{x}'$ , an optimal solution to the constrained surrogate function is the same as the result by MIHT. In addition, we get the following inequality

$$-\|\mathbf{Ax}'^{t+1} - \mathbf{Ax}'\|_2^2 + \frac{1}{2\eta} \|\mathbf{x}'^{t+1} - \mathbf{x}'\|_2^2 \geq (-\|\mathbf{A}\|_2^2 + \frac{1}{2\eta}) \|\mathbf{x}'^{t+1} - \mathbf{x}'\|_2^2. \quad (\text{G.6})$$

When  $\eta < 1/(2\|\mathbf{A}\|_2^2)$ , we have

$$-\|\mathbf{Ax}'^{t+1} - \mathbf{Ax}'\|_2^2 + \frac{1}{2\eta} \|\mathbf{x}'^{t+1} - \mathbf{x}'\|_2^2 \geq 0, \quad (\text{G.7})$$

where the equal sign holds if and only if  $\mathbf{x}'^{t+1} = \mathbf{x}'$ . In accordance to (G.1), (G.5) and (G.7), with  $\eta < 1/(2\|\mathbf{A}\|_2^2)$ , we obtain

$$f(\mathbf{x}') = \varepsilon(\mathbf{x}', \mathbf{x}') \geq \varepsilon(\mathbf{x}'^{t+1}, \mathbf{x}') \geq f(\mathbf{x}'^{t+1}). \quad (\text{G.8})$$

The proof is complete. ■

## Appendix H. Proof of Theorem 4

Based on (G.8), we have

$$f(\mathbf{x}') \geq f(\mathbf{x}'^{t+1}) - \|\mathbf{Ax}'^{t+1} - \mathbf{Ax}'\|_2^2 + \frac{1}{2\eta} \|\mathbf{x}'^{t+1} - \mathbf{x}'\|_2^2 \quad (\text{H.1a})$$

$$\Rightarrow f(\mathbf{x}') \geq f(\mathbf{x}'^{t+1}) + \left( \frac{1}{2\eta} - \|\mathbf{A}\|_2^2 \right) \|\mathbf{x}'^{t+1} - \mathbf{x}'\|_2^2. \quad (\text{H.1b})$$

That is, with  $0 < \eta < 1/(2\|\mathbf{A}\|_2^2)$  and  $\|\mathbf{x}'\|_2 < +\infty$ , if  $\|\mathbf{x}'^{t+1}\|_2 \rightarrow +\infty$ , we have  $\|\mathbf{x}'^{t+1} - \mathbf{x}'\|_2^2 \rightarrow +\infty$ , resulting in  $f(\mathbf{x}') \rightarrow +\infty$ .

For Property (ii), since  $\mathbf{x}' \in \mathcal{C}$ ,  $\mathbf{x}'$  is bounded.

We then prove Property (iii). From (H.1b), we obtain:

$$\left( \frac{1}{2\eta} - \|\mathbf{A}\|_2^2 \right) \|\mathbf{x}'^{t+1} - \mathbf{x}'\|_2^2 \leq f(\mathbf{x}') - f(\mathbf{x}'^{t+1}) \quad (\text{H.2})$$

By induction on  $t$ , we have

$$\left(\frac{1}{2\eta} - \|\mathbf{A}\|_2^2\right) \sum_{t=1}^T \|\mathbf{x}^{t+1} - \mathbf{x}^t\|_2^2 \leq f(\mathbf{x}^1) - f(\mathbf{x}^{T+1}). \quad (\text{H.3})$$

Since  $\{f(\mathbf{x}^t)\}_{t=1}^\infty$  is convergent, (H.3) leads to

$$\lim_{T \rightarrow \infty} \sum_{t=1}^T \|\mathbf{x}^{t+1} - \mathbf{x}^t\|_2^2 < +\infty, \quad (\text{H.4a})$$

$$\Rightarrow \lim_{T \rightarrow \infty} \|\mathbf{x}^{t+1} - \mathbf{x}^t\|_2 = 0. \quad (\text{H.4b})$$

From (H.4b) and the boundedness of  $\{\mathbf{x}^t\}_{t=1}^\infty$ , given  $\mathbf{x}^1$ ,  $\{\mathbf{x}^t\}_{t=1}^\infty$  has convergent subsequences, and each of them has its limit.

Now, we apply proof by contradiction to show that all the limits for a given  $\mathbf{x}^1$  are the same. If  $\{\mathbf{x}^t\}_{t=1}^\infty$  has at least two different limits, then  $\{f(\mathbf{x}^t)\}_{t=1}^\infty$  has at least two different limits due to  $f(\mathbf{x}^{t+1}) < f(\mathbf{x}^t)$  with  $\mathbf{x}^{t+1} \neq \mathbf{x}^t$ . This contradicts with the fact that  $\{f(\mathbf{x}^t)\}_{t=1}^\infty$  converges. For example, if  $\{\mathbf{x}^t\}_{t=1}^\infty$  has two different limits, namely,  $\mathbf{x}^*$  and  $\mathbf{x}^{**}$ , then as  $t \rightarrow \infty$ ,  $f(\mathbf{x}^t)$  will alternatively change between  $f(\mathbf{x}^*)$  and  $f(\mathbf{x}^{**})$ . This behavior contradicts with Theorem 3 that  $\{f(\mathbf{x}^t)\}_{t=1}^\infty$  is convergent.

To sum up,  $\{\mathbf{x}^t\}_{t=1}^\infty$  has one limit, indicating  $\{\mathbf{x}^t\}_{t=1}^\infty$  is convergent. The proof is complete. ■

## References

- [1] D.L. Donoho, Compressed sensing, *IEEE Trans. Inf. Theory* 52 (4) (2006) 1289–1306.
- [2] E.J. Candès, J. Romberg, T. Tao, Robust uncertainty principles: exact signal reconstruction from highly incomplete frequency information, *IEEE Trans. Inf. Theory* 52 (2) (2006) 489–509.
- [3] H. Liu, J. Peng, Z. Lin, A theoretical result of sparse signal recovery via alternating projection method, *Inf. Sci.* 506 (2020) 51–57.
- [4] X.-P. Li, Z.-L. Shi, L. Huang, A.M.-C. So, H.C. So, Rocs: robust one-bit compressed sensing with application to direction of arrival, *IEEE Trans. Signal Process.* (2024) (Early Access).
- [5] L. Feng, H. Sun, J. Zhu, Robust image compressive sensing based on half-quadratic function and weighted schatten-p norm, *Inf. Sci.* 477 (2019) 265–280.
- [6] C. Bao, H. Ji, Y. Quan, Z. Shen, Dictionary learning for sparse coding: algorithms and convergence analysis, *IEEE Trans. Pattern Anal. Mach. Intell.* 38 (7) (2015) 1356–1369.
- [7] M. Lustig, D.L. Donoho, J.M. Santos, J.M. Pauly, Compressed sensing MRI, *IEEE Signal Process. Mag.* 25 (2) (2008) 72–82.
- [8] M.A. Herman, T. Strohmer, High-resolution radar via compressed sensing, *IEEE Trans. Signal Process.* 57 (6) (2009) 2275–2284.
- [9] T. Guha, R.K. Ward, Learning sparse representations for human action recognition, *IEEE Trans. Pattern Anal. Mach. Intell.* 34 (8) (2012) 1576–1588.
- [10] C. Yang, Y. Gu, B. Chen, H. Ma, H.C. So, Learning proximal operator methods for nonconvex sparse recovery with theoretical guarantee, *IEEE Trans. Signal Process.* 68 (2020) 5244–5259.
- [11] R. Jansen, R. Van Dijk, Optimal benchmark tracking with small portfolios, *J. Portf. Manag.* 28 (2) (2002) 33–39.
- [12] Y. Feng, D.P. Palomar, A signal processing perspective on financial engineering, *Found. Trends Signal Process.* 9 (1/2) (2016) 1–231.
- [13] J.M. Bioucas-Dias, A. Plaza, N. Dobigeon, M. Parente, Q. Du, P. Gader, J. Chanussot, Hyperspectral unmixing overview: geometrical, statistical, and sparse regression-based approaches, *IEEE J. Sel. Top. Appl. Earth Obs. Remote Sens.* 5 (2) (2012) 354–379.
- [14] K.J. Oh, T.Y. Kim, S. Min, Using genetic algorithm to support portfolio optimization for index fund management, *Expert Syst. Appl.* 28 (2) (2005) 371–379.
- [15] X.P. Li, Z.-L. Shi, C.-S. Leung, H.C. So, Sparse index tracking with k-sparsity or  $\epsilon$ -deviation constraint via  $\ell_0$ -norm minimization, *IEEE Trans. Neural Netw. Learn. Syst.* (2022) 1–14, Early Access.
- [16] N. Gillis, S.A. Vavasis, Fast and robust recursive algorithms for separable nonnegative matrix factorization, *IEEE Trans. Pattern Anal. Mach. Intell.* 36 (4) (2014) 698–714.
- [17] T.T. Nguyen, J. Idier, C. Soussen, E.-H. Djermoune, Non-negative orthogonal greedy algorithms, *IEEE Trans. Signal Process.* 67 (21) (2019) 5643–5658.
- [18] F.-Y. Wu, K. Yang, Y. Hu, Sparse estimator with  $\ell_0$ -norm constraint kernel maximum-correntropy-criterion, *IEEE Trans. Circuits Syst. II, Express Briefs* 67 (2) (2019) 400–404.
- [19] E.J. Candès, X. Li, Y. Ma, J. Wright, Robust principal component analysis?, *J. ACM* 58 (3) (2011) 1–37.
- [20] Z. Li, H. Zhao, Y. Guo, Z. Yang, S. Xie, Accelerated log-regularized convolutional transform learning and its convergence guarantee, *IEEE Trans. Cybern.* 52 (10) (2021) 10785–10799.
- [21] L.R. Sant'Anna, J.F. Caldeira, T.P. Filomena, LASSO-based index tracking and statistical arbitrage long-short strategies, *N. Am. J. Econ. Finance* 51 (2020) 101055.
- [22] R. Tibshirani, Regression shrinkage and selection via the lasso, *J. R. Stat. Soc., Ser. B, Methodol.* 58 (1) (1996) 267–288.
- [23] F.E. Harrell, *Regression Modeling Strategies: with Applications to Linear Models, Logistic and Ordinal Regression, and Survival Analysis*, Springer, 2015.
- [24] M.-D. Iordache, J.M. Bioucas-Dias, A. Plaza, Sparse unmixing of hyperspectral data, *IEEE Trans. Geosci. Remote Sens.* 49 (6) (2011) 2014–2039.
- [25] M.-D. Iordache, J. Bioucas-Dias, A. Plaza, Total variation spatial regularization for sparse hyperspectral unmixing, *IEEE Trans. Geosci. Remote Sens.* 50 (11) (2012) 4484–4502.
- [26] S. Zhang, J. Li, H.-C. Li, C. Deng, A. Plaza, Spectral-spatial weighted sparse regression for hyperspectral image unmixing, *IEEE Trans. Geosci. Remote Sens.* 56 (6) (2018) 3265–3276.
- [27] H. Zou, The adaptive lasso and its oracle properties, *J. Am. Stat. Assoc.* 101 (476) (2012) 1418–1429.
- [28] L. Shu, F. Shi, G. Tian, High-dimensional index tracking based on the adaptive elastic net, *Quant. Finance* (2020) 1–18.
- [29] Y. Zheng, T.M. Hospedales, Y. Yang, Diversity and sparsity: a new perspective on index tracking, in: *IEEE Int. Conf. Acoust. Speech Signal Process. (ICASSP)*, Barcelona, Spain, 2020, pp. 1768–1772.
- [30] R. Andreani, E.G. Birgin, J.M. Martínez, M.L. Schuverdt, On augmented Lagrangian methods with general lower-level constraints, *SIAM J. Optim.* 18 (4) (2008) 1286–1309.
- [31] K. Benidis, Y. Feng, D.P. Palomar, Optimization methods for financial index tracking: from theory to practice, *Found. Trends Optim.* 3 (3) (2018) 171–279.
- [32] K. Benidis, Y. Feng, D.P. Palomar, Sparse portfolios for high-dimensional financial index tracking, *IEEE Trans. Signal Process.* 66 (1) (2018) 155–170.
- [33] D.R. Hunter, MM algorithms for generalized Bradley-Terry models, *Ann. Stat.* 32 (1) (2004) 384–406.
- [34] F.-Y. Wu, K. Yang, R. Duan, Compressed sensing of underwater acoustic signals via structured approximation  $\ell_0$ -norm, *IEEE Trans. Veh. Technol.* 67 (9) (2018) 8504–8513.
- [35] F.-Y. Wu, K. Yang, Z. Yang, Compressed acquisition and denoising recovery of EMGdi signal in WSNs and IoT, *IEEE Trans. Ind. Inform.* 14 (5) (2017) 2210–2219.
- [36] C. Li, Y. Liu, J. Cheng, R. Song, J. Ma, C. Sui, X. Chen, Sparse unmixing of hyperspectral data with bandwise model, *Inf. Sci.* 512 (2020) 1424–1441.
- [37] P.H. Calamai, J.J. Moré, Projected gradient methods for linearly constrained problems, *Math. Program.* 39 (1) (1987) 93–116.
- [38] C.-J. Lin, Projected gradient methods for nonnegative matrix factorization, *Neural Comput.* 19 (10) (2007) 2756–2779.

- [39] N. Parikh, S. Boyd, Proximal algorithms, *Found. Trends Optim.* 1 (3) (2014) 127–239.
- [40] S. Boyd, L. Vandenberghe, *Convex Optimization*, Cambridge Univ. Press, 2004.
- [41] Y. Sun, P. Babu, D.P. Palomar, Majorization-minimization algorithms in signal processing, communications, and machine learning, *IEEE Trans. Signal Process.* 65 (3) (2016) 794–816.
- [42] M.-F. Leung, J. Wang, Minimax and biobjective portfolio selection based on collaborative neurodynamic optimization, *IEEE Trans. Neural Netw. Learn. Syst.* 32 (7) (2020) 2825–2836.
- [43] G. Guastaroba, M.G. Speranza, Kernel search: an application to the index tracking problem, *Eur. J. Oper. Res.* 217 (1) (2012) 54–68.
- [44] J.M. Bioucas-Dias, M.A. Figueiredo, Alternating direction algorithms for constrained sparse regression: application to hyperspectral unmixing, in: 2nd Workshop Hyperspectral Image Signal Process. Evol. Remote Sens., Reykjavik, Iceland, 2010, pp. 1–4.
- [45] R.A. Borsoi, T. Imbiriba, J.C.M. Bermudez, C. Richard, A fast multiscale spatial regularization for sparse hyperspectral unmixing, *IEEE Geosci. Remote Sens. Lett.* 16 (4) (2019) 598–602.
- [46] B. Somers, M. Zortea, A. Plaza, G.P. Asner, Automated extraction of image-based endmember bundles for improved spectral unmixing, *IEEE J. Sel. Top. Appl. Earth Obs. Remote Sens.* 5 (2) (2012) 396–408.